Key factors affecting single scattering albedo calculation: Implications for aerosol climate forcing

Duseong S. Jo[1, a, b], Rokjin J. Park[1, *], Jaein I. Jeong[1], Gabriele Curci[2], Hyung-Min Lee[3, c],

and Sang-Woo Kim[1]

[1]School of Earth and Environmental Science, Seoul National University, Seoul, Republic of Korea

[2]Department of Physical and Chemical Sciences, Center of Excellence for the Forecast of Severe Weather (CETEMPS), University of L'Aquila, L'Aquila, Italy

[3]Department of Civil, Environmental, and Architectural Engineering, University of Colorado, Boulder, CO, USA

[a]now at Cooperative Institute for Research in Environmental Sciences, University of Colorado, Boulder, CO, USA

[b]now at Department of Chemistry and Biochemistry, University of Colorado, Boulder, CO, USA

[c]now at School of Earth and Environmental Science, Seoul National University, Seoul, Republic of Korea

*Correspondence to: R. J. Park (rjpark@snu.ac.kr)

Abstract

Single Scattering Albedo (SSA), the ratio of scattering efficiency to total extinction efficiency, is an essential parameter used to estimate the Direct Radiative Forcing (DRF) of aerosols. However, SSA is one of the large contributors to the uncertainty of DRF

5   estimations. In this study, we examined the sensitivity of SSA calculations to the physical properties of absorbing aerosols, in particular, Black Carbon (BC), Brown Carbon (BrC), and dust. We used GEOS-Chem 3-D global chemical transport model (CTM) simulations and a post-processing tool for the aerosol optical properties (FlexAOD). The model and input parameters were evaluated by comparison against the observed aerosol mass concentrations

10 and the Aerosol Optical Depth (AOD) values obtained from global surface observation networks such as the global Aerosol Mass Spectrometer (AMS) dataset, the Surface Particulate Matter Network (SPARTAN), and the Aerosol Robotic Network (AERONET). The model was generally successful in reproducing the observed variability of both the Particulate Matter 2.5 μm ($PM_{2.5}$) and AOD (R ~ 0.76) values, although it underestimated the

15 magnitudes by approximately 20 %. Our sensitivity tests of the SSA calculation revealed that the aerosol physical parameters, which have generally received less attention than the aerosol mass loadings, can cause large uncertainties in the resulting DRF estimation. For example, large variations in the calculated BC absorption may result from slight changes of the geometric mean radius, geometric standard deviation, real and imaginary refractive indices,

20 and density. The inclusion of BrC and observationally-constrained dust size distributions also significantly affected the SSA, and resulted in a remarkable improvement for the simulated SSA at 440 nm (bias was reduced by 44 – 49 %) compared with the AERONET observations. Based on the simulations performed during this study, we found that the global aerosol direct radiative effect was increased by 10 % after the SSA bias was reduced.

1   Introduction

Aerosol Optical Depth (AOD), Single Scattering Albedo (SSA), and asymmetry

parameters are important inputs used for calculating the Direct Radiative Forcing (DRF) of

aerosols (Iacono et al., 2008). Among aerosol optical properties, the SSA is the factor that

5   most contributes to the uncertainty of the aerosol DRF calculations. Previous studies have

suggested that a small change in the SSA can lead to a significant change in the aerosol

radiative forcing based on the analysis of in-situ observations, chemical transport and

radiative transfer model results, and satellite data (Loeb and Su, 2010; McComiskey et al.,

2008; Srivastava et al., 2011). For example, a decrease in the SSA from 0.9 to 0.8 (an 11 %

10   decrease) can often change the sign of the DRF from negative (cooling), to positive

(warming) values (Jethva et al., 2014).

Generally, the aerosol SSA is calculated using the Mie theory by assuming the

particles are spherical. This spherical assumption may not be applicable to aerosols that have

diverse geometrical shapes such as Black Carbon (BC) and soil dust (Mishchenko, 2009). For

15   this reason, previous studies have suggested alternative methods such as the Rayleigh-Debye-

Gans theory for aggregates (Farias et al., 1996), and the T-matrix method for non-spherical

particles (Mishchenko, 2009). However, the Mie theory is still a powerful tool for global

model calculations by virtue of its brevity, computational efficiency, and applicability to

radiative transfer models. As a result, in a recent Aerosol Comparisons between Observations

20   and Models (AeroCom) study (Myhre et al., 2013b), which was the basis of the fifth

assessment report from the Intergovernmental Panel on Climate Change (IPCC) (Myhre et

al., 2013a), Mie theory was used in all of the participating models.

The application of Mie theory for aerosol SSA calculations requires precise

information about the size distribution, refractive index, particle density, and hygroscopic

growth factors of aerosols. However, it is difficult to determine these parameters from

measurements because the characteristics of aerosols vary widely depending on the region,

source, aging and mixing state, and measurement technique. As a result, the input parameters

used for aerosol SSA calculations are variable and depend on the corresponding

5   measurements, which can cause a wide range of calculated aerosol SSAs. For example, some

previous global modeling studies found that no significant bias existed between calculated

SSAs versus Aerosol Robotic Network (AERONET) observations (Chin et al., 2009; Dai et

al., 2015), while other studies showed positive biases in the estimates (Feng et al., 2013; Jo et

al., 2016; Lin et al., 2014; Myhre et al., 2009). We surmised that the SSA bias could be

10   reduced when models use relatively high BC emissions and a low BC density. For example,

Chin et al. (2009), used a BC emission of 10.2 TgC yr^{-1}, which is 50 % higher than the 6.8

TgC yr^{-1} used by Jo et al. (2016) and a BC density of 1.0 g cm^{-3}, which is the lowest value

used in the literature (Koch et al., 2009). Since there is limited information available on the

emission and physical parameters of the BC values used in previous studies, we cannot reach

15   a conclusion that explains the range of global SSA values that have been estimated by

previous modeling studies. Instead, we mainly focused on the physical parameters affecting

the SSA calculation, which are discussed below.

Choosing the appropriate input parameters for Mie calculations is a greater challenge

for BC than for other aerosols, because BC particles usually exist as agglomerates of primary

20   spherules rather than individual spherical particles (Alexander et al., 2008). As a result, the

physical parameters for BC used in the AeroCom models are variable for the mass median

diameter (0.020 – 0.852 μm), density (1.0 – 2.0 g cm^{-3}), and refractive indices (1.75 – 0.44i –

2.0 – 1.0i) (Koch et al., 2009). Furthermore, the SSA may vary significantly depending on the

mixing state. Both theoretical and observational studies showed that an SSA value of an

internally mixed BC aerosol is lower than that of an externally mixed BC (Bond et al., 2006; Drury et al., 2010; Shiraiwa et al., 2008).

Although BC is a major species contributing to aerosol absorption, soil dust is also an important contributor (Yang et al., 2009). The global mass concentration of soil dust is the

5 largest amongst the other aerosols. Thus, soil dust could have a significant impact on the global SSA, especially since the size distributions of dust are poorly evaluated in global models (Kok, 2011; Kok et al., 2017). Previous studies showed a significant change in the observed SSA (Khatri et al., 2014) and simulated aerosol DRF (Mahowald et al., 2014) as a function of the coarse/fine fractions of soil dust.

10 Finally, few models consider the absorbing fraction of Organic Aerosols (OA), which are typically assumed to be a scattering aerosol, although recent studies have confirmed the presence of this component (Alexander et al., 2008; Kirchstetter and Thatcher, 2012; Laskin et al., 2015). The inclusion of the absorbing OA (known as Brown Carbon, BrC) may have a significant effect on the SSA calculation (Feng et al., 2013; Jo et al., 2016; Lin et al., 2014).

15 In this study, we focused our analysis on four factors, the physical parameters of BC, mixing state, dust size distributions, and the presence of BrC. We conducted global simulations for the years 2008 – 2010 using a 3-D chemical transport model (GEOS-Chem). First, we extensively evaluated the simulated aerosol mass concentrations and aerosol optical properties by comparing the model with observations from global aerosol observation

20 networks such as the global Aerosol Mass Spectrometer (AMS) dataset, the Surface Particulate Matter Network (SPARTAN), and AERONET for the years 2008 – 2010. Multiple sensitivity simulations were also carried out to examine the effects of individual factors on the calculated SSA as discussed above. Finally, using the simulation results, we estimated the aerosol Direct Radiative Effect (DRE) and its sensitivity to the assumed factors, to provide

insights in the climatic implications of current Global Climate Models (GCMs).

2   Model description

We used the GEOS-Chem (version 10.1) global 3-D chemical transport model (Bey et

5   al., 2001), which is driven by the Modern Era Retrospective-analysis for Research and

Applications (MERRA) assimilated meteorological data from the Global Modeling and

Assimilation Office (GMAO) (Rienecker et al., 2011). Meteorological data including

temperature, wind, humidity, planetary boundary layer height, and other meteorological

variables at 0.5° x 0.667° horizontal resolutions were re-gridded to 2° x 2.5° for this study.

10   We conducted an NO_x-O_x-hydrocarbon-aerosol full chemistry simulation, including

BC, OA, SO_4^{2-}, NO_3^-, NH_4^+, soil dust, and sea salt aerosols. BC and OA were simulated

based on the work published by Park et al. (2003). The model simulated BC and Primary OA

(POA), with a hydrophobic and a hydrophilic tracer for each. For a Secondary OA (SOA)

simulation, we used the scheme developed by Pye et al. (2010), which considers the parent

15   hydrocarbons of monoterpenes, sesquiterpenes, isoprene, and aromatics with NO_x dependent

yields. SOA was considered as hydrophilic, and further details are described in Pye et al.

(2010).

For the sensitivity study described in Section 3.4, we additionally considered BrC by

using the BrC/OC ratio calculated by Jo et al. (2016). We applied the BrC/OC ratio to the

20   simulated POA and SOA of each grid box in order to calculate the BrC from both primary

and secondary sources. The ratio of BrC to OC burden was 0.19 across the globe, but could

be regionally variable as shown in Figure 7 in Jo et al. (2016). The detailed BrC estimation

method and the global distributions are described in Jo et al. (2016).

The model simulated inorganic aerosols following the method of Park et al. (2004).

Nitrate aerosol formation was computed using ISORROPIA II (Fountoukis and Nenes, 2007;

Pye et al., 2009), which calculates the H_2SO_4-HNO_3-NH_3-H_2O thermodynamics. Dust

aerosols were simulated using the Dust Entrainment And Deposition (DEAD) scheme of

Zender et al. (2003), along with the source function used in GOCART (Ginoux et al., 2001),

5   as presented by Fairlie et al. (2007). The sea salt emission was estimated as a function of dry

particle size, local 10 m wind speed, and sea surface temperature (Alexander et al., 2005;

Jaeglé et al., 2011).

We used the anthropogenic emission values of BC, OC, CO, NO_x, NH_3, and SO_2 from

the Hemispheric Transport of Air Pollution (HTAP) v2 inventory with a horizontal resolution

10   of 0.1° x 0.1° (Janssens-Maenhout et al., 2015). HTAP v2 includes ships, energy, industry,

transport, residential, and agriculture sector data. For NH_3, we applied the diurnal variation

factors from Zhu et al. (2015) in order to reduce the high bias of nitrate aerosol simulations.

Aircraft emission values were considered by using the Aviation Emissions Inventory Code

(AEIC) database (Stettler et al., 2011). Anthropogenic emissions of hydrocarbons including

15   benzene, toluene, and xylene were taken from the Reanalysis of the Tropospheric chemical

composition (RETRO) inventory (Schultz et al., 2007). Biogenic VOC emissions were taken

from the Model of Emissions of Gases and Aerosols from Nature (MEGAN) v2.1 (Guenther

et al., 2012). The emissions of the VOCs were computed on the basis of emission activity

factors, soil moisture, leaf age, and canopy environment. The Global Fire Emission Database

20   version 4 (GFEDv4) inventory (Giglio et al., 2013) was used for biomass burning emissions

at a 0.25° x 0.25° spatial resolution. The global emission values used in this study are

summarized in Table 1.

3   Aerosol optical property calculation

3.1 FlexAOD

We calculated the AOD, SSA, and asymmetry parameters using the Flexible Aerosol

Optical Depth (FlexAOD) tool, which is a GEOS-Chem post-processing tool for aerosol

5   optical property calculations (Curci et al., 2015). FlexAOD uses Mie theory (Mishchenko et

al., 2002) with input data including size distributions, refractive indices, particle density, and

hygroscopic growth factors included for each aerosol species. Aerosol mixing state and its

effects on the AOD, SSA, and asymmetry parameter were also considered. We assumed three

different mixing states - external mixing, homogeneous internal mixing, and core-shell

10   internal mixing. Each aerosol was assumed to be formed by a single chemical species in the

case of external mixing. Homogeneous internal mixing assumes that all aerosols are well

mixed, and the core-shell internal mixing assumes that an insoluble well-mixed core is coated

by a concentric well-mixed soluble shell. A detailed description of the aerosol optical

property calculation with different mixing states can be found in Section 2 of Curci et al.

15   (2015).

3.2 Input parameters for FlexAOD

Table 2 summarizes the input parameters used in the Mie calculation of FlexAOD.

The values in Table 2 are the same as the input parameters used in online aerosol optical

property and photolysis rate calculations in the standard GEOS-Chem v10.1. Input

20   parameters in GEOS-Chem were initially taken from the Optical Properties of Aerosols and

Clouds (OPAC) database (Hess et al., 1998) and Chin et al. (2002), as described in Martin et

al. (2003).

Herein, we briefly discuss the significant updates to the method of Martin et al. (2003)

that we used in this study. The log-normal distribution was assumed for aerosols except for

soil dust, which follow the Gamma distribution. The geometric standard deviations of the

inorganic aerosols, OA, and BC were reduced from 2.0 (OPAC) to 1.6 based on

measurements from the optical particle counter instrument during the International

Consortium for Atmospheric Research on Transport and Transformation (ICARTT) 2004

5   field campaign (Drury et al., 2010). Inorganic aerosols followed the refractive index and

hygroscopic growth factors (HGFs) of water-soluble component (WASO), which were

changed from those of sulfate droplets (SUSO) in OPAC. HGFs of OA were updated to 1.35

at 95 % RH based on the chamber and field observations of Jimenez et al. (2009). The

geometric mean radius of BC was 0.020 μm, which was increased from 0.012 μm. The

10   density of BC was increased to 1.8 g cm^{-3} (Bond and Bergstrom, 2006) from 1.0 g cm^{-3} by

OPAC (Hess et al., 1998). These BC-related parameter changes led to significant changes in

aerosol absorption, which are discussed in the following section.

3.3 Effects of size distribution and refractive index of BC on absorption

As discussed in Section 1, BC particles typically form aggregates (Alexander et al.,

15   2008), which makes it difficult to choose the appropriate BC radius in the Mie calculation

(Koch et al., 2009). Here we examined the sensitivity of BC absorption with respect to the

choice of geometric mean radius (r_g) and geometric standard deviation (σ) using Mie theory.

Using a BC column concentration of 0.25 mg m^{-2} we calculated the Absorption AOD

(AAOD) for 1 – 200 nm (r_g) and 1.2, 1.6, and 2.0 (σ) as shown in Figure 1(a). Values were

20   generally within the reported ranges of global mean BC AAODs (0.8 X 10^{-3} – 3.5 X 10^{-3})

from the AeroCom phase Ⅰ models, although we did not consider hygroscopic growth. Red

star and blue rectangle symbols indicate OPAC values (r_g = 12 nm and σ = 2.0) and GEOS-

Chem default size distributions (r_g = 20 nm and σ = 1.6). We found that the use of these two

size distributions led to very similar AAODs (< 1 % difference), resulting from the combined

effects of the increased r_g and decreased σ.

Figure 1(b) represents the calculated BC AAOD values as a function of real and imaginary refractive indices. BC AAOD values increased as the imaginary refractive index increased and the real refractive index decreased. Red star and blue triangles indicate BC

5   AAOD values using the refractive indices from OPAC (1.74 – 0.44i) and Bond and Bergstrom (2006) (1.95 – 0.79i), respectively. BC AAOD values using refractive indices between 1.95 – 0.79i were 49 % higher than the values obtained using refractive indices between 1.74 – 0.44i. A similar result was reported by Stier et al. (2007), who also found that their AAOD values when using refractive indices between 1.95 – 0.79i were 52 % higher

10   than those found using 1.74 – 0.44i in the ECHAM5-HAM model.

3.4 FlexAOD simulations

Using the aerosol mass concentrations from the GEOS-Chem simulations above, we carried out a number of FlexAOD simulations by changing the input parameters. Here we focused on BC because of its high contribution to light absorption and the diverse

15   morphologies found in the atmosphere (Alexander et al., 2008). We examined the sensitivity of the calculated aerosol absorption to the assumed input parameters shown in Table 3. For example, the GEOS case indicates a FlexAOD simulation using GEOS-Chem default values as of v10-01. The OPAC database was used for the OP sensitivity case. Refractive indices between 1.95 – 0.79i were used for BB, BBR, and BBHR cases with different geometric

20   radiuses of BC (Table 3). The geometric mean radius of 0.065 μm was adapted from Bond et al. (2013). We additionally assumed a geometric mean radius of 0.1 μm, which seemed to be higher than that used by previous studies (Bond et al., 2013; Wang et al., 2014), however, the value was still within the range of the AeroCom study (Koch et al., 2009).

After the sensitivity simulations shown in Table 3, we further considered different

mixing states, the effects of brown carbon, and also the observationally constrained dust size distributions. We added tag names for representing these factors. As discussed in Section 3.1, we considered the three mixing states of external, homogeneous internal, and core-shell internal and the corresponding "_E", "_H", and "_C" tag names were added to base case

5 names in Table 3, respectively. If the sensitivity case includes BrC absorption, the "_BR" tag name was added. We also implemented a new dust size distribution in the model as suggested by Zhang et al. (2013). Zhang et al. (2013), developed the dust size distribution with constraints from in-situ measurements and the work of Kok (2011), who suggested new dust size distributions based on the physics of the scale-invariant fragmentation of brittle

10 materials. The "_DI" tag name was applied when we used the dust size distribution by Zhang et al. (2013). For instance, "GEOS_BR_DI_H" indicates that the model with GEOS-Chem default input parameters, brown carbon, dust size distribution by Zhang et al. (2013), and the homogeneous internal mixing assumption were used.

15 **4   Model evaluations**

4.1 Global aerosol mass concentration

We used the AMS dataset (Zhang et al., 2007) and the SPARTAN observations (Snider et al., 2015) to evaluate the simulated mass concentrations of aerosols globally. Since the observations were available for multiple years (AMS: 2000 ~ 2008, SPARTAN: 2013 ~

20 2015), we focused our evaluation on the observed monthly variation using the monthly mean value of the simulation averaged for the years 2008 – 2010. Year to year variability was not considered in this study similar to previous studies (Jo et al., 2013; Spracklen et al., 2011; Yu, 2011).

Figure 2 shows point-to-point comparisons of the simulated monthly mean sulfate,

nitrate, ammonium, and organic aerosol concentrations with the AMS network observations.

Statistical parameters including the regression slope, y-intercept (Y-ict), correlation

coefficient (R), normalized mean bias (NMB), and root mean square error (RMSE) are

presented in Table 4. We found that the model successfully reproduced the observed

5   inorganic aerosol concentrations with correlation coefficients of 0.62 – 0.78 and regression

slopes of 0.69 – 0.84. Compared to Jo et al. (2013), the model showed an improved

performance in terms of statistics (e. g. RMSEs were decreased by 22 – 45 %). These

improvements are attributed to the different emission inventory values used in this study.

In contrast to inorganic aerosols, the model showed a low correlation coefficient

10   (0.36) and a high RMSE (4.77 µg m^{-3}) for OA. This result is consistent with the evaluation of

OA against AMS found previously in the literature (Jo et al., 2013; Yu, 2011). The low bias (-

37 %) in the model was mainly caused by poor SOA simulations, which still showed a

considerable gap from observations as pointed out by the recent AeroCom inter-comparison

study for OA (Tsigaridis et al., 2014).

15   Figure 3 shows the scatter plots of BC, sulfate, nitrate, ammonium, dust, and

Particulate Matter with a radius of 2.5 μm (PM$_{2.5}$) between SPARTAN observations and the

model results. Statistical parameters are also shown in Table 4. We found that the model

performance for inorganic aerosols was degraded, especially for nitrate aerosols. Differences

in values between observation years is one of the reasons for the discrepancy between the

20   AMS (2000 – 2008) and the SPARTAN (2013 – 2015) dataset model evaluations. During the

past decade, NO$_x$ emissions and column concentrations over the United States and Europe

have been decreasing (Curier et al., 2014; Granier et al., 2011; Simon et al., 2014), and the

United States and Europe are the main regions covered by the AMS observation network

(Zhang et al., 2007). Therefore, there is a possibility that these two different global

observation networks (AMS and SPARTAN) represent different nitrate concentration levels.
We found that the nitrate overestimation mainly occurred over the United States (7 of 19
points above 10:1 line in Figure 3) and South Asia (7 of 19 points above 10:1 line in Figure
3). The nitrate overestimation of GEOS-Chem is consistently reported in previous studies for

5 the United States (Heald et al., 2012; Schiferl et al., 2014; Zhang et al., 2012; Zhu et al.,
2013), South Asia (Gu and Liao, 2015), and East Asia (Wang et al., 2013). There have been
some efforts to find the possible cause of the nitrate overestimation (e. g. the uptake
efficiency of N_2O_5 on aerosols, the reaction rate for the formation of nitric acid, dry
deposition velocity, boundary layer height, and the uptake of nitric acid on coarse mode dust

10 or sea salt), but this issue is not still resolved (Heald et al., 2012; Zhang et al., 2012; Zhu et
al., 2013). Photolysis of nitrate also can reduce the overestimation as recently observed by Ye
et al. (2017). An investigation of nitrate overestimation is beyond the scope of this study, and
will be conducted in future studies.

Compared to nitrate, the BC values showed a relatively better result with a regression

15 slope of 0.94. However, the BC concentration was underestimated by 37 %, and the
underestimation occurred mainly in Manila (10 of 13 points below 10:1 line in Figure 3). We
found that the model grid box corresponding to this site was mostly oceanic (Figure S1). The
spatial resolution of the model (2° x 2.5°) was too coarse to capture local sources on the
island.

20 For the comparison of dust, we inferred the observed dust mass concentrations
following the SPARTAN speciation of Snider et al. (2016). They calculated the dust mass by
multiplying [Al + Fe + Mg] by 10 based on the elemental composition of natural dust
presented by Wang (2015). Although this calculation seems oversimplified, we found that the
method of Snider et al. (2016) was similar to the method of Malm et al. (1994) for estimating

dust mass concentrations based on the observed trace metal concentrations (regression slope of 1.0 and correlation of 0.98).

Simulated PM$_{2.5}$ concentrations were generally in good agreement with the observations (R = 0.76) with a slight low bias observed for the mean concentrations (-24 %).

5   The performance of the model was comparable to that of global PM$_{2.5}$ estimates constrained by using satellite AOD observations (R = 0.73 – 0.81 and regression slopes of 0.68 – 0.96) (van Donkelaar et al., 2015), which provides confidence in the model's ability to reproduce the AOD and SSA values.

4.2 AOD and SSA

10   The model appeared to appropriately capture the spatial and temporal (monthly) variability of the observed PM$_{2.5}$ described above. This may result from the combination of the nitrate overestimation and the OA underestimation. To ensure the reliability of the model for the AOD and the SSA evaluation in this section, we also selected simulated results at AERONET sites, which met the following criteria: (1) Differences between the monthly

15   mean observed and simulated concentrations of each aerosol species (inorganics, OA, BC, and dust) should be less than a factor of two at surface networks (AMS and SPARTAN). (2) AERONET and AMS (or SPARTAN) sites should be in the same model grid or adjacent model grids. We could have applied stricter criteria for our data selection, but too few data were available for the analysis. Our conclusions, however, were found not to be sensitive to

20   the criteria used as discussed below.

Figure 4(a) shows the scatterplot of the simulated versus observed AOD at 500 nm using the base case (GEOS_E). We found that the statistics of the AOD evaluation were very similar to that of the PM$_{2.5}$. The slopes were 0.68 and 0.70, the correlation coefficient was 0.76, and the Normalized Mean Biases (NMBs) were -20 % and -24 %, for AOD and PM$_{2.5}$,

respectively. From this result, we concluded that the aerosol optical property calculation in FlexAOD was properly performed. When we filtered out data at AERONET sites using the criteria above, the model showed improved statistics against the observations. The NMB was reduced to -10 %, and the correlation coefficient was increased to 0.82 (Figure 4(b)).

5   Figure 5(a) and 5(b) are point to point comparisons of the SSA with all AERONET sites for 440 nm and 870 nm. Here we excluded SSA values when the AOD was less than 0.4 because the AERONET SSA retrieval showed high uncertainty for low AOD conditions (Dubovik et al., 2002). The model appropriately simulated the SSA at 870 nm in common with the evaluation of the AOD at 500 nm, but significantly overestimated the observed SSA

10 at 440 nm. The SSA of the model (0.949) was higher than that of the AERONET (0.897) by 0.052. In other words, the model underestimated the observed absorption (1-SSA) by -50 %. Although the model underestimated BC by -37 %, the model also underestimated scattering aerosols (PM$_{2.5}$ minus BC) by -23 %. Therefore, the SSA overestimation could be caused by other factors than the underestimation of the BC mass concentration. This overestimation is

15 similar to the result by Jo et al. (2016), who also found significant SSA overestimation of the GEOS-Chem version 9.1.2 against AERONET. The reasons for this overestimation will be investigated in following sections.

        Figure 5(c) and 5(d) represent comparison results similar to Figure 5(a, b) but use only selected data. The model showed an improved result especially for the SSA at 440 nm.

20 The correlation was increased to 0.5 from 0.34, which is analogous to the evaluated result of the AOD at 500 nm. From these results, we concluded that the model simulation capability of the AOD and SSA was improved when we selected AERONET sites where the model showed good results against the AMS and SPARTAN network. Hereafter, we used these selected AERONET sites for the sensitivity studies below.

5   SSA sensitivity

In this section, we present the sensitivity analysis of the calculated SSA values for three factors including the aerosol mixing states, the inclusion of BrC, and dust size distributions. The sensitivity of the BC physical properties were also investigated but did not

5   show significant differences (Figure S2). We compared the calculated values against the observed SSA at 440 and 870 nm from AERONET sites across the globe. We thoroughly examined the statistics of the simulated values versus the observed SSA for the ensemble of AERONET sites in this section in order to determine the best parameters for the global SSA estimation.

10   The effects of the BC internal mixing on the SSA calculation are shown in Figure 6. We found that both homogeneous (Figure 6(a)) and core-shell (Figure 6(b)) internal mixing assumptions led to a significant decrease of the SSA (0.842 – 0.851) at 440 nm. Furthermore, the NMBs of the AOD were decreased to -52 % with the internal mixing cases (GEOS_H and GEOS_C) from -10 % with the external mixing case (GEOS_E) (Table S1). The decreased

15   internal mixing AODs compared to the external mixing decreased by -34 – -37 % because of the decrease of the aerosol numbers with the increased size of each aerosol, which is consistent with previously published results by Curci et al. (2015).

The inclusion of the BrC absorption (GEOS_BR_E) and the use of the dust size distribution presented by Zhang et al. (2013) (GEOS_DI_E) also reduced the SSA

20   overestimation (Figure 6(c-d)). The mean SSAs were decreased by 0.008 – 0.015. The regression slope also increased from 0.38 to between 0.55 – 0.67. The correlation slightly increased for the GEOS_BR_E case (0.56), but decreased for the GEOS_DI_E case as a result of the more widely scattered points that were affected by high dust concentrations. In contrast to the internal mixing results above, the AOD was not significantly decreased (-7 %

– 1 %) with respect to the GEOS_E case.

Figure 7 shows the combined effects of both the BrC absorption and the dust size distribution on the 440 nm SSA calculation. All four sensitivity cases showed improved results although the overestimation of the SSA still existed in the model. We speculate that

5   this remaining gap could be reduced when we consider strongly absorbing BrC as some studies have reported (Alexander et al., 2008; Chung et al., 2012). However, it is too uncertain whether the strongly absorbing BrC is dominant globally. The reported BrC absorptions vary by two orders of magnitude (Jo et al., 2016) and further studies are needed to clarify the presence of strongly absorbing BrC.

10   On the other hand, we found that the correlation coefficients and regression slopes decreased as the radius of BC increased. We surmised that the use of a spherule size radius (~0.02 μm) seemed more appropriate than the aggregate size radius (~0.1 μm) for the calculations using Mie theory. However, the result can be affected by many factors, and therefore it is difficult to generalize the use of the radius in this study.

15   Contrary to the comparisons of the SSA at 440 nm, the model showed different results for the SSA at 870 nm (Figure 8). Aerosol absorption at 870 nm is mainly affected by BC rather than BrC and dust (Yang et al., 2009). Therefore, the differences are mainly attributed to the size distributions and the refractive indices of the BC. Since BC is the only contributor to aerosol absorption at 870 nm, we found that the effects of the BC refractive index on the

20   SSA were more important for the 870 nm than for the 440 nm results. The 870 nm SSA decreased by the use of higher refractive index (BB_BR_DI_E - GEOS_BR_DI_E) was -0.017, the absolute magnitude of which is larger than the 440 nm SSA decrease of -0.011 (Table 6).

Considering all the evaluations for the AOD and SSA above, we found that the

GEOS_BR_DI_E case showed the best performance against AERONET observations. In the following section, we used this case for the DRE calculation and calculated the effects of the sensitivity factors on the DRE change.

6   Implication for global DRE

Here we calculated the global clear-sky DRE of selected sensitivity simulations in Figure 9 by using the Rapid Radiative Transfer Model for General Circulation Models (RRTMGs) (Iacono et al., 2008). MERRA reanalysis data were used for albedo and other meteorological variables.

Figure 9(a) shows the annual mean DRE of the reference simulation (GEOS_E) for the years 2008 – 2010. Globally, annual mean DREs are negative except for Northern Africa where weakly absorbing dust concentrations were very high. The absolute magnitudes of the DRE were high in regions with heavy biomass burning (Central Africa) and anthropogenic (East Asia) emissions. These global distributions are similar to the results presented by Heald et al. (2014) (Figure 3 in their paper). The annual mean DRE was -2.62 W m^{-2}, which is also comparable to the annual mean DRE (-2.75 W m^{-2}) for 2010 published by Heald et al. (2014).

The inclusion of the BrC absorption increased the DRE by 0.07 W m^{-2}, especially for regions with high biomass burning (Africa) and biofuel (Asia) emissions (Jo et al., 2016) as shown in Figure 9(e). Note that the BrC absorption could be underestimated in this study as discussed in Section 5, and in turn, the DRE increased by BrC could be underestimated. The DRE increase after modifying the dust size distribution was 0.17 W m^{-2} (Figure 9(f)), which is more than two times higher than the DRE increase by BrC absorption. When we considered both the BrC absorption and the observationally constrained dust size distribution, the increment of the DRE was 0.26 W m^{-2} (Figure 9(g)), which accounts for 10 % of the DRE

of the reference case.

The inclusion of the BrC absorption (-0.015) led to a more effective decrease of the

SSA at 440 nm than the change of dust size distribution (-0.008) as shown in Table 5.

However, the effects on the DRE were different. The relatively higher DRE change (0.17 W

5   m^{-2}) shown in Figure 9(f) is mainly caused by high dust burden (14.4 Tg), which was 10 –

100 times higher than the BC (0.1 Tg), or OA (1.4 Tg) burden. Note that the DRE is

calculated by using the AOD (~proportional to burden) as well as the SSA. Therefore, we

conclude that the size distribution of dust plays an important role in the modelled DRE

estimation, as also reported by Kok et al. (2017).

7   Conclusions

Although we found that the GEOS_BR_DI_E case showed the best performance

against the AERONET AOD and SSA, it is difficult to confirm whether this result can be

applied to other studies. There were many factors simultaneously affecting the AOD and SSA

15   calculation such as the hygroscopic growth factor, which was not discussed in detail.

However, we were able to identify some notable findings that could apply to future modeling

studies when using Mie theory for the calculation of aerosol optical properties:

1. There were no significant differences between the calculated BC absorptions using input

parameters from the OPAC database and data from Bond and Bergstrom (2006). The

20   refractive indices used by Bond and Bergstrom (2006) (1.95 – 0.79i) were higher than those

used by OPAC (1.74 – 0.44i), and the resulting BC absorption of Bond and Bergstrom (2006)

was 49 % higher than that of OPAC. However, the low BC particle density of OPAC (1.0 g

cm^{-3}) increased the BC number concentration and the AOD, which enhanced the BC

absorption. We found that the mean SSA of OP_E (0.927) was slightly lower than that of

BB_E (0.934) (Table 5). Although many previous studies did not provide the BC density they used for the Mie calculation (Feng et al., 2013; Jo et al., 2016; Lin et al., 2014), an assumed BC density was critical to the SSA calculation and should be provided in future inter-comparison studies.

5   2. The model using the external mixing assumption showed better performance than the model using internal mixing assumptions in a global modeling sense. Drury et al. (2010), also showed similar results against aircraft observations. The internal mixing assumptions caused very high absorption and an underestimation of the AERONET SSA. The effect of internal mixing on absorption could be overestimated in the model calculations; Cappa et al. (2012)

10   reported that the observed ambient BC absorption enhancements obtained by internal mixing were small (~6 %), which is less than predicted from theoretical calculations and observed from laboratory measurements. Furthermore, BC absorption enhancement by internal mixing could vary by region (Liu et al., 2015). Coating thickness could also be different due to aging timescales and the distance of source regions. Further observational and modeling studies are

15   needed especially for considering region-specific absorption enhancement.

3. The modelled SSA calculations from previous studies were mostly evaluated between 440 – 550 nm (Dai et al., 2015; Jo et al., 2016; Lin et al., 2014). However, SSAs at both shorter and longer wavelengths should be evaluated together for the model evaluation. The calculated SSA could show different performances at different wavelengths because they are affected by

20   different aerosols and wavelength-dependent physical characteristics.

4. BrC absorption and observationally constrained dust size distributions should be considered for the SSA calculation in the model, especially for the shorter wavelengths. These factors reduced the SSA at shorter wavelengths, resulting in a decrease of the positive SSA bias at 440 nm generally found in global models.

5. The changes of dust size distribution led to a significant increase of the global DRE, whose value (0.17 W m^{-2}) was more than two times higher than the global DRE increase by BrC absorption (0.07 W m^{-2}). Global models likely underestimate the global dust DRE because of the overestimation of fine mode dust and the underestimation of the coarse mode dust as

5 shown by Kok et al. (2017), who constrained the global dust size distribution using global observations and models.

Acknowledgements

We would like to thank the SPARTAN project for establishing and maintaining the

10 SPARTAN sites used in this investigation. The SPARTAN network was initiated with funding from the Natural Sciences and Engineering Research Council of Canada. We thank the principal investigators and their staff for establishing and maintaining the AERONET sites used in this study. We also want to thank Q. Zhang and D. V. Spracklen for providing the global AMS data. This study was supported by the Korea Ministry of Environment as

15 "Climate Change Correspondence Program" and "Public Technology Program based on Environmental Policy" (2017000160001).

Table 1. Global emission values from 2008 to 2010 used in this study.

Emission type	Species								Source
	NOₓ [TgN yr⁻¹]	SOₓ [TgS yr⁻¹]	NH₃ [TgN yr⁻¹]	BC [TgC yr⁻¹]	OC [TgC yr⁻¹]	Dust [Tg yr⁻¹]	Sea salt [Tg yr⁻¹]		
Anthropogenic	30.0	55.0	39.3[1)	5.5	12.1				HTAPv2
Biomass burning	4.3	0.9	3.3	1.9	16.2				GFEDv4 (Gigilio et al., 2013)
Volcanic		13.9							AEROCOM SO₂ (Diehl et al., 2012)
Oceanic DMS		16.8							Park et al. (2004)
Lightning	7.1								Murray et al. (2012)
Soil	10.2								Hudman et al. (2012)
Aircraft	0.8	0.1							AEIC (Stettler et al., 2011)
Dust						1165.2			DEAD (Fairlie et al., 2007)
Sea salt							3321.8		Jaegle et al. (2011)
Total	52.5	86.7	42.6	7.4	28.3	1165.2	3321.8		

1) Including agriculture sector.

Table 2. Input parameters used in the Mie calculation for FlexAOD. The log-normal distribution with geometric mean radius (r_g) and geometric standard deviation (σ_g) are assumed for aerosols except for dust, which follows the gamma distribution with gamma A and gamma B. Particle density (ρ), refractive index (RI), and hygroscopic growth factors (HGF) are also presented.

				Sea salt		Dust			
	Inorganics	OA	BC	Accumulation	Coarse	Bin1 (0.1~1.0 μm)	Bin2 (1.0~1.8 μm)	Bin3 (1.8~3.0 μm)	Bin4 (3.0~6.0 μm)
r_g (μm)	0.0695[a]	0.073[b]	0.020[e]	0.085[g]	0.401[g]				
σ_g	1.6[b]	1.6[b]	1.6[b]	1.5[g]	1.8[g]				
Gamma							A = 0.9, B = 0.2		
ρ (g cm^{-3})	1.7[c]	1.8[a]	1.8[f]	2.2[a]		2.5	2.65	2.65	2.65
RI at 550 nm	1.53 - 0.006i[a]	1.53 - 0.006i[a]	1.74 - 0.44i[a]	1.50 - 10^{-8}i[a]			1.558 - 0.0014i[h]		
HGF at 50%	1.34[a]	1.14[d]	1.0[c]	1.81[a]	1.81[a]		1.0	1.0	
HGF at 95%	1.88[a]	1.35[d]	1.50[c]	2.89[a]	2.92[a]				

a) OPAC (Hess et al., 1998)
b) Drury et al. (2010)
c) GOCART (Chin et al., 2002)
d) Jimenez et al. (2009)
e) http://wiki.seas.harvard.edu/geos-chem/index.php/Aerosol_optical_properties#Overview
f) Bond and Bergstrom (2006)
g) Jaegle et al. (2011)
h) Sinyuk et al. (2003)

Table 3. Sensitivity simulation input parameters of BC cases used in this study.

Case	Refractive index	Mean Radius [μm]	Sigma	Density [g cm^{-3}]
GEOS	1.74 - 0.44i	0.02	1.6	1.8
OP	1.74 - 0.44i	0.0118	2.0	1.0
BB	1.95 - 0.79i	0.02	1.6	1.8
BBR	1.95 - 0.79i	0.065	1.6	1.8
BBHR	1.95 - 0.79i	0.1	1.6	1.8

Table 4. Statistical parameters for the evaluation of the model against global aerosol mass concentration observation networks. Regressions slopes and Y-intercepts were computed using the reduced-major-axis method (Hirsch and Gilroy, 1984).

Network	Species	Slope	Y-ict	R	NMB	RMSE
AMS	Sulfate	0.77	1.31	0.78	0.17	2.25
	Nitrate	0.84	0.68	0.62	0.40	2.04
	Ammonium	0.69	0.71	0.78	0.21	1.18
	Organics	0.59	0.18	0.36	-0.37	4.77
SPARTAN	BC	0.94	-0.80	0.47	-0.37	2.20
	Sulfate	0.75	1.02	0.48	-0.05	3.84
	Nitrate	3.60	0.45	0.68	2.92	7.66
	Ammonium	1.72	0.48	0.59	1.01	3.03
	Dust	1.14	-1.88	0.38	-0.25	6.00
	PM$_{2.5}$	0.70	2.37	0.76	-0.24	21.65

Table 5. Statistical parameters for the comparison between the simulated and the observed SSA at 440 nm for AOD > 0.4. The observed mean SSA was 0.888.

Cases	Slope	Yict	R	RMSE	Mean	Mean bias
GEOS_E	0.38	0.60	0.50	0.061	0.944	0.057
OP_E	0.53	0.45	0.52	0.045	0.927	0.039
BB_E	0.45	0.53	0.53	0.051	0.934	0.046
BBR_E	0.38	0.61	0.49	0.061	0.944	0.057
BBHR_E	0.39	0.61	0.38	0.069	0.952	0.064
GEOS_H	2.18	-1.08	0.13	0.070	0.851	-0.037
GEOS_C	2.03	-0.96	0.14	0.072	0.842	-0.045
OP_H	2.98	-1.83	0.07	0.110	0.812	-0.076
OP_C	2.53	-1.43	0.09	0.099	0.817	-0.071
GEOS_BR_E	0.55	0.44	0.56	0.046	0.929	0.041
GEOS_DI_E	0.67	0.34	0.34	0.055	0.936	0.049
GEOS_BR_DI_E	0.70	0.30	0.53	0.039	0.920	0.032
BB_BR_DI_E	0.75	0.24	0.57	0.031	0.909	0.021
BBR_BR_DI_E	0.69	0.31	0.52	0.039	0.920	0.032
BBHR_BR_DI_E	0.68	0.32	0.46	0.047	0.928	0.040

Table 6. Statistical parameters for the comparison between the simulated and the observed SSA

at 870 nm for AOD > 0.4. The observed mean SSA was 0.918.

Cases	Slope	Yict	R	RMSE	Mean	Mean bias
GEOS_E	1.17	-0.16	0.76	0.026	0.923	0.005
OP_E	1.63	-0.60	0.77	0.041	0.898	-0.020
BB_E	1.45	-0.42	0.77	0.033	0.908	-0.010
BBR_E	1.49	-0.46	0.77	0.035	0.904	-0.014
BBHR_E	1.35	-0.33	0.77	0.029	0.912	-0.006
GEOS_H	1.58	-0.56	0.70	0.043	0.898	-0.020
GEOS_C	1.83	-0.81	0.73	0.063	0.871	-0.047
OP_H	2.09	-1.05	0.72	0.071	0.868	-0.050
OP_C	2.28	-1.25	0.74	0.093	0.843	-0.075
GEOS_BR_E	1.16	-0.14	0.76	0.025	0.923	0.005
GEOS_DI_E	1.15	-0.14	0.79	0.024	0.913	-0.005
GEOS_BR_DI_E	1.10	-0.10	0.79	0.024	0.909	-0.009
BB_BR_DI_E	1.37	-0.37	0.79	0.038	0.892	-0.026
BBR_BR_DI_E	1.41	-0.40	0.80	0.041	0.889	-0.029
BBHR_BR_DI_E	1.27	-0.27	0.80	0.033	0.897	-0.021
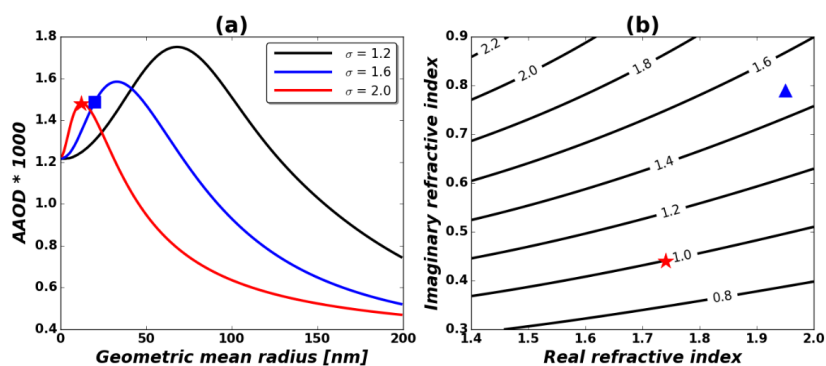
Figure 1. (a) Calculated BC AAOD at 550 nm (y-axis) as a function of geometric mean radius (r_g) [nm] (x-axis). Three different geometric standard deviations (σ) are assumed – 1.2 (black line), 1.6 (blue line), and 2.0 (red line). Red star and blue rectangle symbols indicate OPAC (r_g = 12 nm and σ = 2.0) and GEOS-Chem default conditions (r_g = 20 nm and σ = 1.6), respectively. Refractive indices of $1.95 - 0.79i$ were used for this calculation. (b) Calculated BC AAOD (multiplied by 1000, contour line) as a function of the real refractive index (x-axis) and the imaginary refractive index (y-axis). Red star and blue triangle symbols represent BC AAODs using refractive indices by OPAC ($1.74 - 0.44i$) and Bond and Bergstrom (2006) ($1.95 - 0.79i$), respectively (r_g of 20 nm and σ of 1.6 were assumed in this calculation). For both plots, a BC column concentration of 0.25 mg m^{-2} and particle density of 1.8 g cm^{-3} were used. Hygroscopic growth was not accounted for in this calculation.
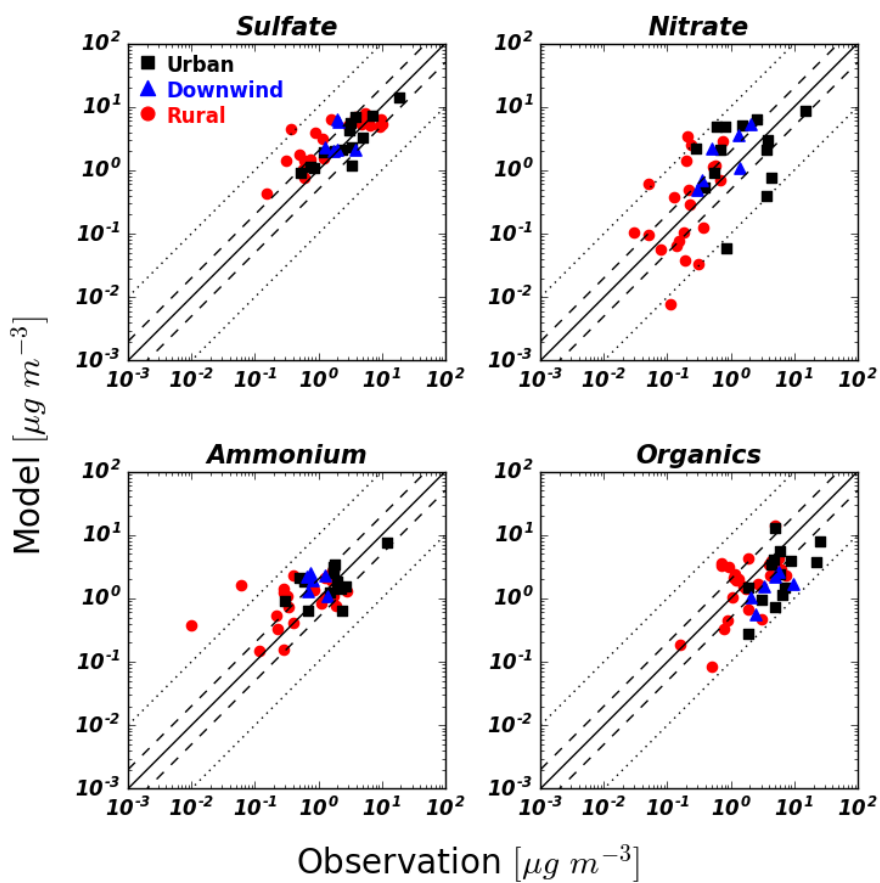
Figure 2. Point-to-point comparisons of the simulated sulfate, nitrate, ammonium, and organics against the AMS network observations. We multiplied the organic matter to organic carbon ratio of 2.1 to organics to account for the non-carbon mass. The 1:1 line (solid), 2:1 lines (dashed), 10:1 lines (dotted) are indicated.
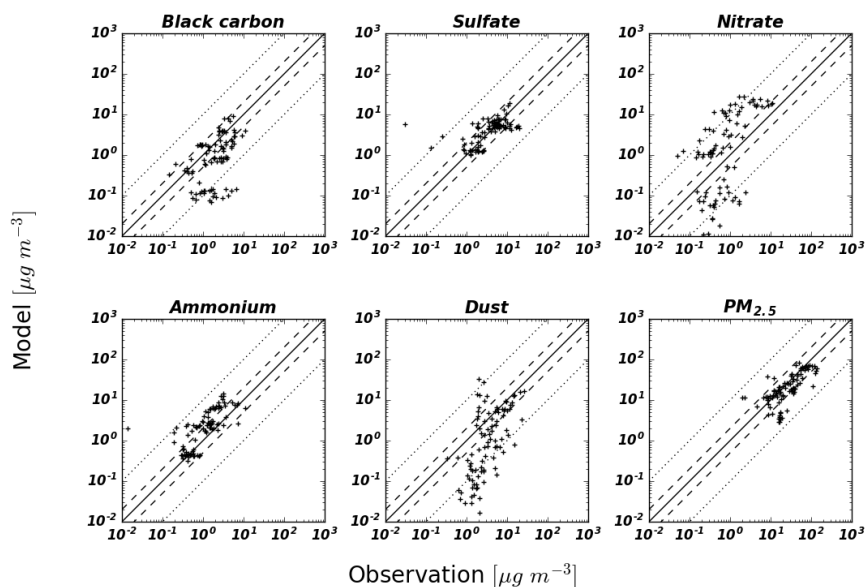
Figure 3. Scatter plots of BC, sulfate, nitrate, ammonium, dust, and PM$_{2.5}$ between SPARTAN observations (x-axis) and the model (y-axis). The 1:1 line (solid), 2:1 lines (dashed), 10:1 lines (dotted) are indicated.
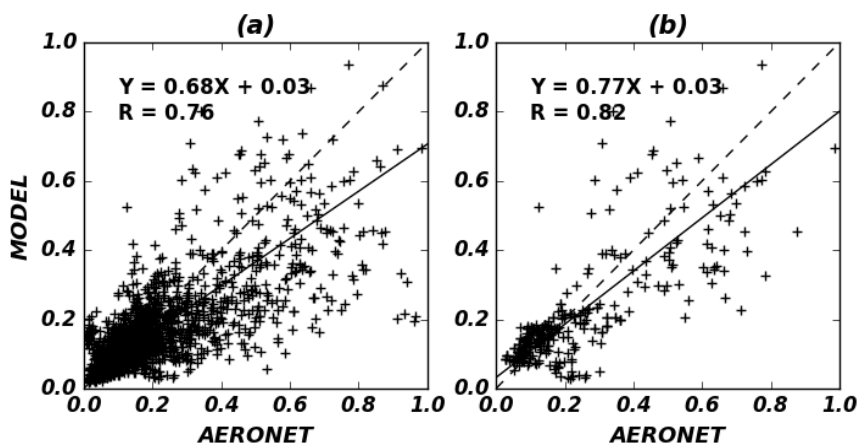
Figure 4. Scatter plot of simulated versus observed AOD at 500 nm from 2008 – 2010 for (a) all AERONET points and (b) AERONET points constrained by model evaluation against the AMS and SPARTAN network. Reduced major axis regression is shown along with the regression equation and R. Each point indicates monthly averaged AOD when the number of observation was greater than 10 days.
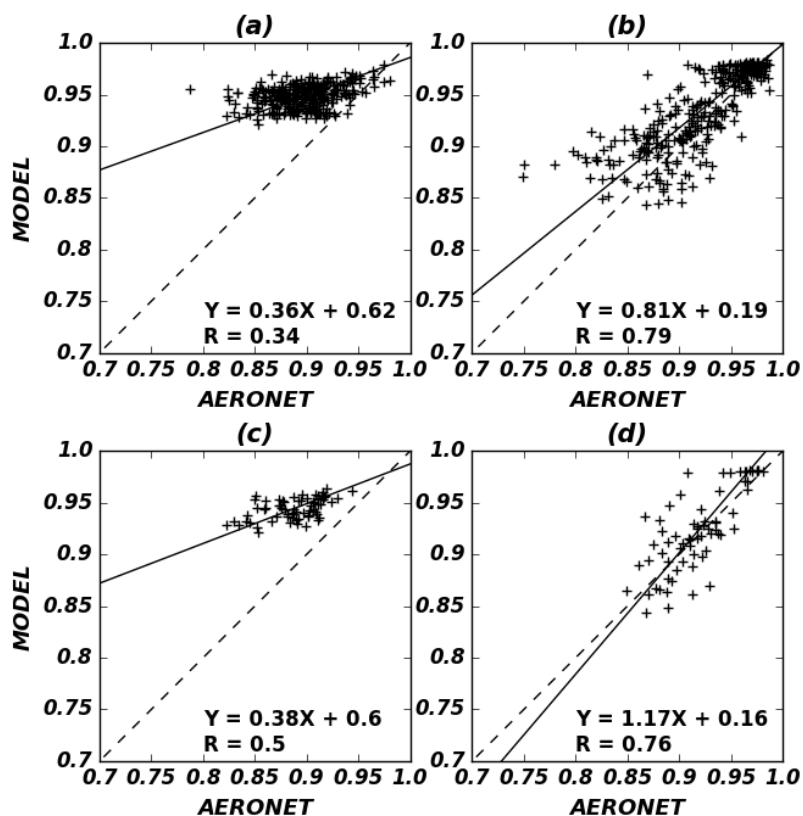
Figure 5. Scatter plots of simulated versus observed SSA at 440 (a, c) and 870 nm (b, d) from
2008 – 2010. All available AERONET sites were used for (a, b) and filtered AERONET sites
were used for (c, d). Reduced major axis regression is shown along with the regression equation
and R. Each point indicates monthly averaged SSA when the number of observation was greater
than 10 days, and AOD at 440 nm was greater than 0.4.
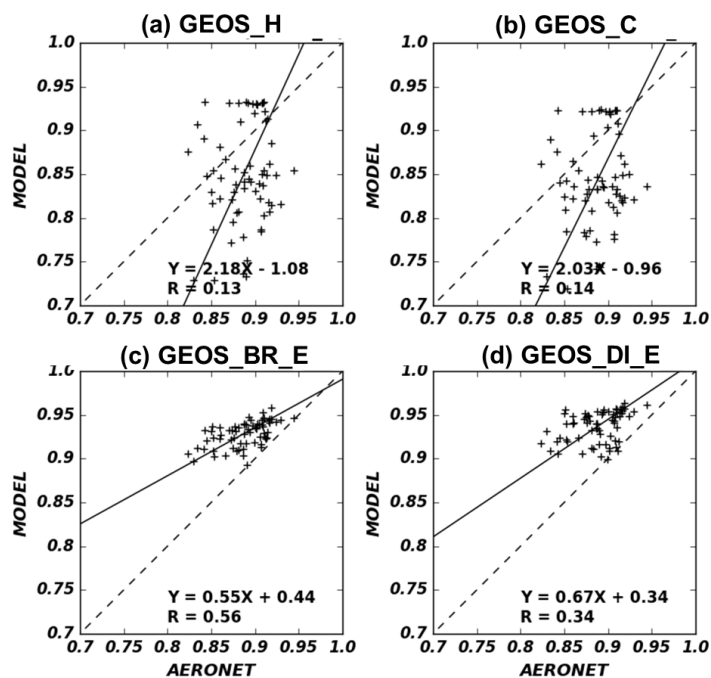
Figure 6. Scatter plots of simulated versus observed SSA at 440 nm for sensitivity simulations
of (a) GEOS_H (Homogeneous internal mixing), (b) GEOS_C (Core-shell internal mixing), (c)
GEOS_BR_E (External mixing with brown carbon absorption), and (d) GEOS_DI_E (External
5   mixing with observationally-constrained dust size distribution).
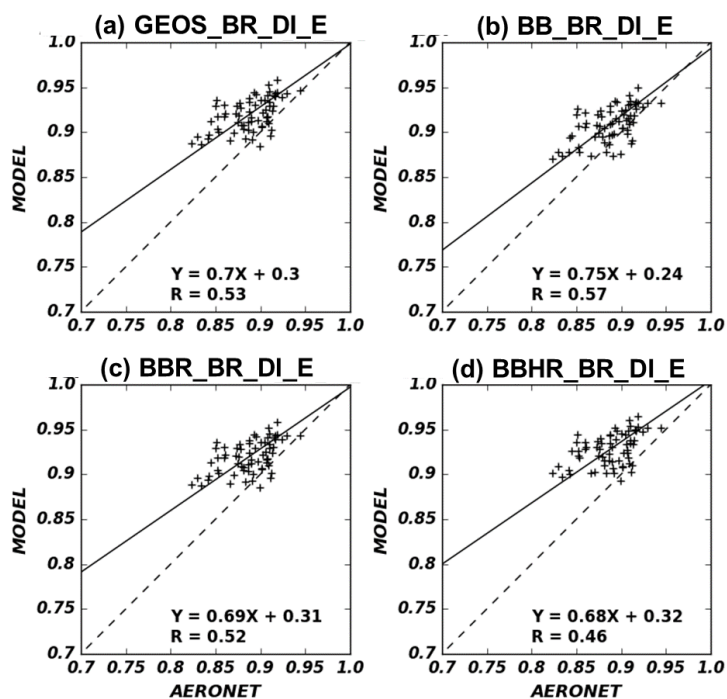
Figure 7. Scatter plots of simulated versus observed SSA at 440 nm for sensitivity simulations of (a) GEOS_BR_DI_E, (b) BB_BR_DI_E, (c) BBR_BR_DI_E, and (d) BBHR_BR_DI_E. GEOS, BB, BBR, and BBHR represent different BC input parameters as described in Table 3. BR_DI_E indicates the external mixing assumption with brown carbon absorption and observationally-constrained dust size distribution.
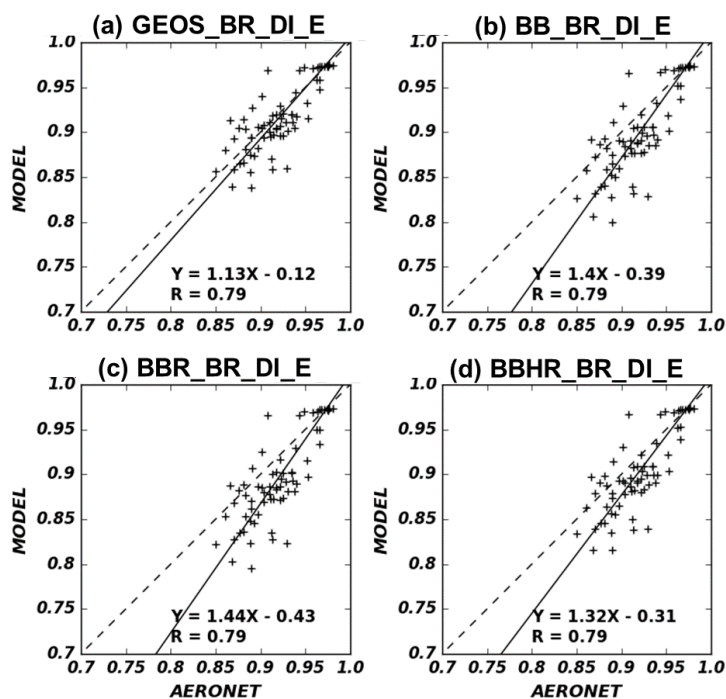
Figure 8. Scatter plots of simulated versus observed SSA at 870 nm for sensitivity simulations
of (a) GEOS_BR_DI_E, (b) BB_BR_DI_E, (c) BBR_BR_DI_E, and (d) BBHR_BR_DI_E.
GEOS, BB, BBR, and BBHR represent different BC input parameters as described in Table 3.
5   BR_DI_E indicates the external mixing assumption with brown carbon absorption and
observationally-constrained dust size distribution.
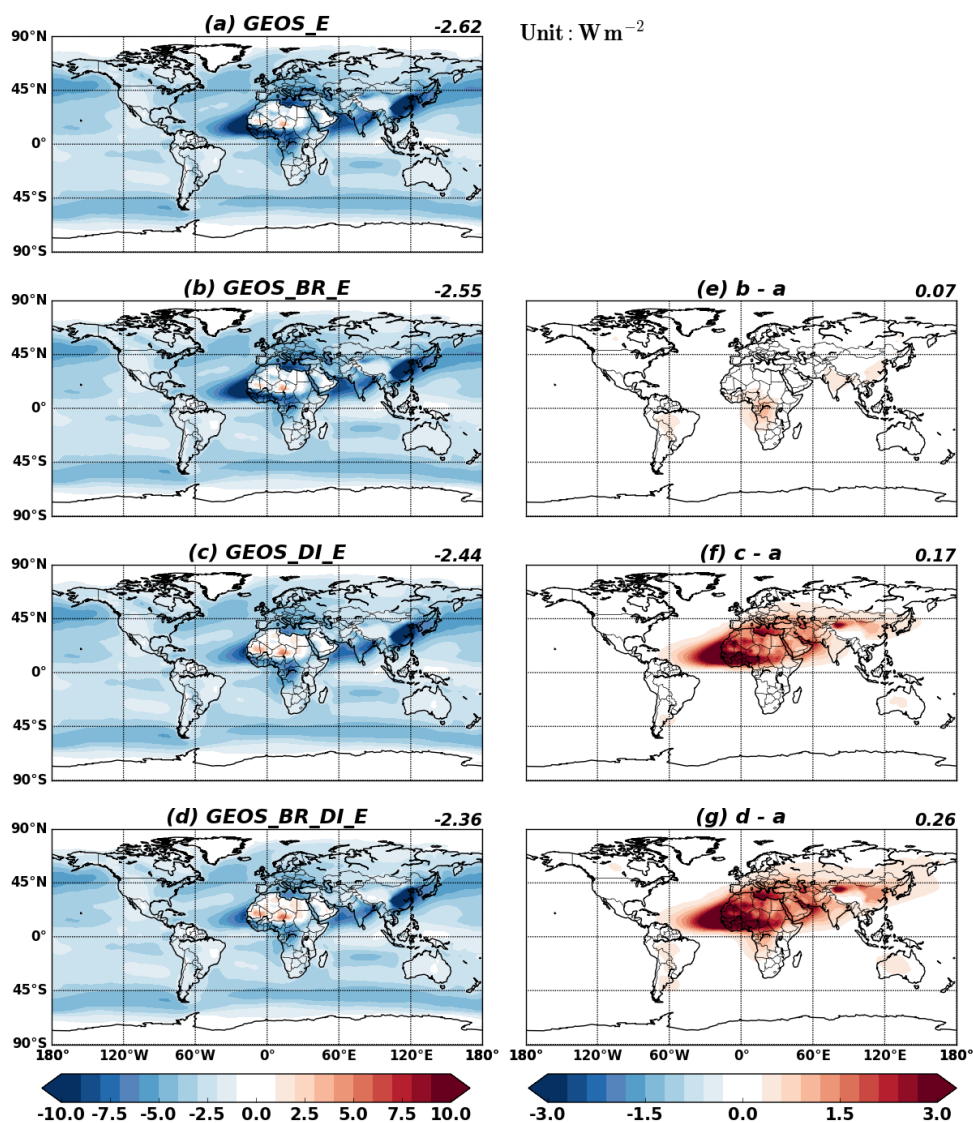
Figure 9. Calculated DREs at the top of the atmosphere. Left panels are the DREs of the (a) GEOS_E, (b) GEOS_BR_E, (c) GEOS_DI_E, and (d) GEOS_BR_DI_E cases. The changes compared with the GEOS_E case are shown in right column.

References

Alexander, B., Park, R. J., Jacob, D. J., Li, Q., Yantosca, R. M., Savarino, J., Lee, C., and Thiemens, M.: Sulfate formation in sea- salt aerosols: Constraints from oxygen isotopes, Journal of Geophysical Research: Atmospheres (1984–2012), 110, 2005.

5 Alexander, D. T. L., Crozier, P. A., and Anderson, J. R.: Brown carbon spheres in East Asian outflow and their optical properties, Science, 321, 833, 2008.

Bey, I., Jacob, D. J., Yantosca, R. M., and Logan, J. A.: Global modeling of tropospheric chemistry with assimilated meteorology- Model description and evaluation, Journal of Geophysical Research, 106, 073-023,095, 2001.

10 Bond, T. C. and Bergstrom, R. W.: Light absorption by carbonaceous particles: An investigative review, Aerosol Science and Technology, 40, 27-67, 2006.

Bond, T. C., Doherty, S. J., Fahey, D. W., Forster, P. M., Berntsen, T., DeAngelo, B. J., Flanner, M. G., Ghan, S., Kärcher, B., Koch, D., Kinne, S., Kondo, Y., Quinn, P. K., Sarofim, M. C., Schultz, M. G., Schulz, M., Venkataraman, C., Zhang, H., Zhang, S., Bellouin, N.,
15 Guttikunda, S. K., Hopke, P. K., Jacobson, M. Z., Kaiser, J. W., Klimont, Z., Lohmann, U., Schwarz, J. P., Shindell, D., Storelvmo, T., Warren, S. G., and Zender, C. S.: Bounding the role of black carbon in the climate system: A scientific assessment, Journal of Geophysical Research, doi: 10.1002/jgrd.50171, 2013. n/a-n/a, 2013.

Bond, T. C., Habib, G., and Bergstrom, R. W.: Limitations in the enhancement of visible light
20 absorption due to mixing state, Journal of Geophysical Research: Atmospheres (1984–2012), 111, 2006.

Cappa, C. D., Onasch, T. B., Massoli, P., Worsnop, D. R., Bates, T. S., Cross, E. S., Davidovits, P., Hakala, J., Hayden, K. L., and Jobson, B. T.: Radiative absorption enhancements due to the mixing state of atmospheric black carbon, Science, 337, 1078-1081,
25 2012.

Chin, M., Diehl, T., Dubovik, O., Eck, T., Holben, B., Sinyuk, A., and Streets, D.: Light absorption by pollution, dust, and biomass burning aerosols: a global model study and evaluation with AERONET measurements, Annales Geophysicae, 27, 3439-3464, 2009.

Chin, M., Ginoux, P., Kinne, S., Torres, O., Holben, B. N., Duncan, B. N., Martin, R. V.,
30 Logan, J. A., Higurashi, A., and Nakajima, T.: Tropospheric Aerosol Optical Thickness from the GOCART Model and Comparisons with Satellite and Sun Photometer Measurements, Journal of Atmospheric Sciences, 59, 461-483, 2002.

Chung, C., Kim, S. W., Lee, M., Yoon, S. C., and Lee, S.: Carbonaceous aerosol AAE inferred from in-situ aerosol measurements at the Gosan ABC super site, and the implications
35 for brown carbon aerosol, Atmospheric Chemistry and Physics, 12, 6173-6184, 2012.

Curci, G., Hogrefe, C., Bianconi, R., Im, U., Balzarini, A., Baró, R., Brunner, D., Forkel, R., Giordano, L., Hirtl, M., Honzak, L., Jiménez-Guerrero, P., Knote, C., Langer, M., Makar, P. A., Pirovano, G., Pérez, J. L., San José, R., Syrakov, D., Tuccella, P., Werhahn, J., Wolke, R., Žabkar, R., Zhang, J., and Galmarini, S.: Uncertainties of simulated aerosol optical properties induced by assumptions on aerosol physical and chemical properties: An AQMEII-2 perspective, Atmospheric Environment, 115, 541-552, 2015.

Curier, R., Kranenburg, R., Segers, A., Timmermans, R., and Schaap, M.: Synergistic use of OMI NO 2 tropospheric columns and LOTOS–EUROS to evaluate the NO x emission trends across Europe, Remote Sensing of Environment, 149, 58-69, 2014.

Dai, T., Shi, G., and Nakajima, T.: Analysis and evaluation of the global aerosol optical properties simulated by an online aerosol-coupled non-hydrostatic icosahedral atmospheric model, Advances in Atmospheric Sciences, 32, 743-758, 2015.

Drury, E., Jacob, D. J., Spurr, R. J., Wang, J., Shinozuka, Y., Anderson, B. E., Clarke, A. D., Dibb, J., McNaughton, C., and Weber, R.: Synthesis of satellite (MODIS), aircraft (ICARTT), and surface (IMPROVE, EPA- AQS, AERONET) aerosol observations over eastern North America to improve MODIS aerosol retrievals and constrain surface aerosol concentrations and sources, Journal of Geophysical Research: Atmospheres (1984–2012), 115, 2010.

Dubovik, O., Holben, B., Eck, T. F., Smirnov, A., Kaufman, Y. J., King, M. D., Tanré, D., and Slutsker, I.: Variability of absorption and optical properties of key aerosol types observed in worldwide locations, Journal of the atmospheric sciences, 59, 590-608, 2002.

Fairlie, T. D., Jacob, D. J., and Park, R. J.: The impact of transpacific transport of mineral dust in the United States, Atmospheric Environment, 41, 1251-1266, 2007.

Farias, T. L., Köylü, Ü. Ö., and Carvalho, M. d. G.: Range of validity of the Rayleigh–Debye–Gans theory for optics of fractal aggregates, Applied Optics, 35, 6560-6567, 1996.

Feng, Y., Ramanathan, V., and Kotamarthi, V.: Brown carbon: a significant atmospheric absorber of solar radiation?, Atmospheric Chemistry and Physics, 13, 8607-8621, 2013.

Fountoukis, C. and Nenes, A.: ISORROPIA II: a computationally efficient thermodynamic equilibrium model for K+-Ca2+-Mg2+-NH4+-Na+-SO42--NO3--Cl--H2O aerosols, Atmospheric Chemistry and Physics Discussions, 7, 1893-1939, 2007.

Giglio, L., Randerson, J. T., and Werf, G. R.: Analysis of daily, monthly, and annual burned area using the fourth- generation global fire emissions database (GFED4), Journal of Geophysical Research: Biogeosciences, 118, 317-328, 2013.

Ginoux, P., Chin, M., Tegen, I., Prospero, J. M., Holben, B., Dubovik, O., and Lin, S. J.: Sources and distributions of dust aerosols simulated with the GOCART model, Journal of Geophysical Research: Atmospheres (1984–2012), 106, 20255-20273, 2001.

Granier, C., Bessagnet, B., Bond, T., D'Angiola, A., Denier van der Gon, H., Frost, G. J., Heil, A., Kaiser, J. W., Kinne, S., and Klimont, Z.: Evolution of anthropogenic and biomass burning emissions of air pollutants at global and regional scales during the 1980–2010 period, Climatic Change, 109, 163-190, 2011.

5   Gu, Y. and Liao, H.: Summertime nitrate aerosol in the upper troposphere and lower stratosphere over the Tibetan Plateau and the South Asian summer monsoon region, Atmospheric Chemistry and Physics Discussions, 15, 32049-32099, 2015.

Guenther, A., Jiang, X., Heald, C., Sakulyanontvittaya, T., Duhl, T., Emmons, L., and Wang, X.: The Model of Emissions of Gases and Aerosols from Nature version 2.1 (MEGAN2. 1):
10   an extended and updated framework for modeling biogenic emissions, Geoscientific Model Development, 5, 1471-1492, 2012.

Heald, C., Collett Jr, J., Lee, T., Benedict, K., Schwandner, F., Li, Y., Clarisse, L., Hurtmans, D., Van Damme, M., and Clerbaux, C.: Atmospheric ammonia and particulate inorganic nitrogen over the United States, Atmospheric Chemistry and Physics Discussions, 12, 19455-
15   19498, 2012.

Heald, C., Ridley, D., Kroll, J., Barrett, S., Cady-Pereira, K., Alvarado, M., and Holmes, C.: Contrasting the direct radiative effect and direct radiative forcing of aerosols, Atmospheric Chemistry and Physics, 14, 5513-5527, 2014.

Hess, M., Koepke, P., and Schult, I.: Optical properties of aerosols and clouds: The software
20   package OPAC, Bulletin of the American meteorological society, 79, 831-844, 1998.

Hirsch, R. and Gilroy, E.: Methods of Fitting a Straight Line to Data: Examples in Water Resources, Water Resources Bulletin, 20, 1984.

Iacono, M. J., Delamere, J. S., Mlawer, E. J., Shephard, M. W., Clough, S. A., and Collins, W. D.: Radiative forcing by long- lived greenhouse gases: Calculations with the AER radiative
25   transfer models, Journal of Geophysical Research: Atmospheres (1984–2012), 113, 2008.

Jaeglé, L., Quinn, P., Bates, T., Alexander, B., and Lin, J.-T.: Global distribution of sea salt aerosols: new constraints from in situ and remote sensing observations, Atmospheric Chemistry and Physics, 11, 3137-3157, 2011.

Janssens-Maenhout, G., Crippa, M., Guizzardi, D., Dentener, F., Muntean, M., Pouliot, G.,
30   Keating, T., Zhang, Q., Kurokawa, J., and Wankmüller, R.: HTAP_v2. 2: a mosaic of regional and global emission grid maps for 2008 and 2010 to study hemispheric transport of air pollution, Atmospheric Chemistry and Physics, 15, 11411-11432, 2015.

Jethva, H., Torres, O., and Ahn, C.: Global assessment of OMI aerosol single- scattering albedo using ground- based AERONET inversion, Journal of Geophysical Research:
35   Atmospheres, 119, 9020-9040, 2014.

Jimenez, J., Canagaratna, M., Donahue, N., Prevot, A., Zhang, Q., Kroll, J., DeCarlo, P., Allan, J., Coe, H., and Ng, N.: Evolution of organic aerosols in the atmosphere, Science, 326, 1525, 2009.

Jo, D., Park, R., Kim, M., and Spracklen, D.: Effects of chemical aging on global secondary organic aerosol using the volatility basis set approach, Atmospheric Environment, 81, 230-244, 2013.

Jo, D. S., Park, R. J., Lee, S., Kim, S. W., and Zhang, X.: A global simulation of brown carbon: implications for photochemistry and direct radiative effect, Atmospheric Chemistry and Physics, 16, 3413-3432, 2016.

Khatri, P., Takamura, T., Shimizu, A., and Sugimoto, N.: Observation of low single scattering albedo of aerosols in the downwind of the East Asian desert and urban areas during the inflow of dust aerosols, Journal of Geophysical Research: Atmospheres, 119, 787-802, 2014.

Kirchstetter, T. and Thatcher, T.: Contribution of organic carbon to wood smoke particulate matter absorption of solar radiation, Atmospheric Chemistry and Physics, 12, 6067-6072, 2012.

Koch, D., Schulz, M., Kinne, S., McNaughton, C., Spackman, J., Balkanski, Y., Bauer, S., Berntsen, T., Bond, T. C., and Boucher, O.: Evaluation of black carbon estimations in global aerosol models, Atmospheric Chemistry and Physics, 9, 9001-9026, 2009.

Kok, J. F.: A scaling theory for the size distribution of emitted dust aerosols suggests climate models underestimate the size of the global dust cycle, Proceedings of the National Academy of Sciences, 108, 1016-1021, 2011.

Kok, J. F., Ridley, D. A., Zhou, Q., Miller, R. L., Zhao, C., Heald, C. L., Ward, D. S., Albani, S., and Haustein, K.: Smaller desert dust cooling effect estimated from analysis of dust size and abundance, Nature Geoscience, 2017. 2017.

Laskin, A., Laskin, J., and Nizkorodov, S. A.: Chemistry of Atmospheric Brown Carbon, Chemical reviews, 115, 4335-4382, 2015.

Lin, G., Penner, J. E., Flanner, M. G., Sillman, S., Xu, L., and Zhou, C.: Radiative forcing of organic aerosol in the atmosphere and on snow: Effects of SOA and brown carbon, Journal of Geophysical Research: Atmospheres, 119, 7453-7476, 2014.

Loeb, N. G. and Su, W.: Direct aerosol radiative forcing uncertainty based on a radiative perturbation analysis, Journal of Climate, 23, 5288-5293, 2010.

Liu, S., Aiken, A. C., Gorkowski, K., Dubey, M. K., Cappa, C. D., Williams, L. R., Herndon, S. C., Massoli, P., Fortner, E. C., and Chhabra, P. S.: Enhanced light absorption by mixed source black and brown carbon particles in UK winter, Nature communications, 6, 2015.

Mahowald, N., Albani, S., Kok, J. F., Engelstaeder, S., Scanza, R., Ward, D. S., and Flanner, M. G.: The size distribution of desert dust aerosols and its impact on the Earth system, Aeolian Research, 15, 53-71, 2014.

Malm, W. C., Sisler, J. F., Huffman, D., Eldred, R. A., and Cahill, T. A.: Spatial and seasonal trends in particle concentration and optical extinction in the United States, Journal of Geophysical Research, 99, 1347-1370, 1994.

Martin, R. V., Jacob, D. J., Yantosca, R. M., Chin, M., and Ginoux, P.: Global and regional decreases in tropospheric oxidants from photochemical effects of aerosols, Journal of Geophysical Research, 108, 4097, 2003.

McComiskey, A., Schwartz, S. E., Schmid, B., Guan, H., Lewis, E. R., Ricchiazzi, P., and Ogren, J. A.: Direct aerosol forcing: Calculation from observables and sensitivities to inputs, Journal of Geophysical Research: Atmospheres, 113, 2008.

Mishchenko, M. I.: Electromagnetic scattering by nonspherical particles: A tutorial review, Journal of Quantitative Spectroscopy and Radiative Transfer, 110, 808-832, 2009.

Mishchenko, M. I., Travis, L. D., and Lacis, A. A.: Scattering, absorption, and emission of light by small particles, Cambridge university press, 2002.

Myhre, G., Berglen, T., Johnsrud, M., Hoyle, C., Berntsen, T., Christopher, S., Fahey, D., Isaksen, I., Jones, T., and Kahn, R.: Modelled radiative forcing of the direct aerosol effect with multi-observation evaluation, Atmospheric Chemistry and Physics, 9, 1365-1392, 2009.

Myhre, G., D. Shindell, F.-M. Bréon, W. Collins, J. Fuglestvedt, J. Huang, D. Koch, J.-F. Lamarque, D. Lee, B. Mendoza, T. Nakajima, A. Robock, G. Stephens, Takemura, T., and Zhang, H.: Anthropogenic and Natural Radiative Forcing. In: Climate Change 2013: The Physical Science Basis. Contribution of Working Group I to the Fifth Assessment Report of the Intergovernmental Panel on Climate Change, Climate change, 2013a. 659-740, 2013a.

Myhre, G., Samset, B., Schulz, M., Balkanski, Y., Bauer, S., Berntsen, T., Bian, H., Bellouin, N., Chin, M., and Diehl, T.: Radiative forcing of the direct aerosol effect from AeroCom Phase II simulations, Atmospheric Chemistry and Physics, 13, 1853-1877, 2013b.

Park, R. J., Jacob, D. J., Chin, M., and Martin, R. V.: Sources of carbonaceous aerosols over the United States and implications for natural visibility, Journal of Geophysical Research, 108, 4355, 2003.

Park, R. J., Jacob, D. J., Field, B. D., Yantosca, R. M., and Chin, M.: Natural and transboundary pollution influences on sulfate-nitrate-ammonium aerosols in the United States: Implications for policy, Journal of Geophysical Research, 109, D15204, 2004.

Pye, H., Chan, A., Barkley, M., and Seinfeld, J.: Global modeling of organic aerosol: the

importance of reactive nitrogen (NO_x and NO_3), Atmospheric Chemistry and Physics, 10, 11261-11276, 2010.

Pye, H. O. T., Liao, H., Wu, S., Mickley, L. J., Jacob, D. J., Henze, D. J., and Seinfeld, J. H.: Effect of changes in climate and emissions on future sulfate-nitrate-ammonium aerosol levels in the United States, Journal of Geophysical Research, 114, 2009.

Rienecker, M. M., Suarez, M. J., Gelaro, R., Todling, R., Bacmeister, J., Liu, E., Bosilovich, M. G., Schubert, S. D., Takacs, L., and Kim, G.-K.: MERRA: NASA's modern-era retrospective analysis for research and applications, Journal of Climate, 24, 3624-3648, 2011.

Schiferl, L. D., Heald, C. L., Nowak, J. B., Holloway, J. S., Neuman, J. A., Bahreini, R., Pollack, I. B., Ryerson, T. B., Wiedinmyer, C., and Murphy, J. G.: An investigation of ammonia and inorganic particulate matter in California during the CalNex campaign, Journal of Geophysical Research: Atmospheres, 119, 1883-1902, 2014.

Schultz, M., Backman, L., Balkanski, Y., Bjoerndalsaeter, S., Brand, R., Burrows, J., Dalsoeren, S., De Vasconcelos, M., Grodtmann, B., and Hauglustaine, D.: REanalysis of the TROpospheric chemical composition over the past 40 years (RETRO)–A long-term global modeling study of tropospheric chemistry, Final Report, Jülich/Hamburg, Germany, 2007. 2007.

Shiraiwa, M., Kondo, Y., Moteki, N., Takegawa, N., Sahu, L., Takami, A., Hatakeyama, S., Yonemura, S., and Blake, D.: Radiative impact of mixing state of black carbon aerosol in Asian outflow, Journal of Geophysical Research: Atmospheres (1984–2012), 113, 2008.

Simon, H., Reff, A., Wells, B., Xing, J., and Frank, N.: Ozone trends across the United States over a period of decreasing NOx and VOC emissions, Environmental science & technology, 49, 186-195, 2014.

Snider, G., Weagle, C., Martin, R., Van Donkelaar, A., Conrad, K., Cunningham, D., Gordon, C., Zwicker, M., Akoshile, C., and Artaxo, P.: SPARTAN: a global network to evaluate and enhance satellite-based estimates of ground-level particulate matter for global health applications, Atmospheric Measurement Techniques, 8, 505-521, 2015.

Snider, G., Weagle, C. L., Murdymootoo, K. K., Ring, A., Ritchie, Y., Stone, E., Walsh, A., Akoshile, C., Anh, N. X., and Balasubramanian, R.: Variation in global chemical composition of PM 2.5: emerging results from SPARTAN, Atmospheric Chemistry and Physics, 16, 9629-9653, 2016.

Spracklen, D. V., Jimenez, J. L., Carslaw, K. S., Worsnop, D. R., Evans, M. J., Mann, G. W., Zhang, Q., Canagaratna, M. R., Allan, J., Coe, H., McFiggans, G., Rap, A., and Forster, P.: Aerosol mass spectrometer constraint on the global secondary organic aerosol budget, Atmospheric Chemistry and Physics., 11, 12109-12136, 2011.

Srivastava, R., Ramachandran, S., Rajesh, T., and Kedia, S.: Aerosol radiative forcing deduced from observations and models over an urban location and sensitivity to single scattering albedo, Atmospheric environment, 45, 6163-6171, 2011.

Stettler, M., Eastham, S., and Barrett, S.: Air quality and public health impacts of UK airports. Part I: Emissions, Atmospheric environment, 45, 5415-5424, 2011.

Stier, P., Seinfeld, J. H., Kinne, S., and Boucher, O.: Aerosol absorption and radiative forcing, Atmospheric Chemistry and Physics, 7, 5237-5261, 2007.

Sinyuk, A., Torres, O., and Dubovik, O.: Combined use of satellite and surface observations to infer the imaginary part of refractive index of Saharan dust, Geophysical Research Letters, 30, 2003.

Tsigaridis, K., Daskalakis, N., Kanakidou, M., Adams, P., Artaxo, P., Bahadur, R., Balkanski, Y., Bauer, S., Bellouin, N., and Benedetti, A.: The AeroCom evaluation and intercomparison of organic aerosol in global models, Atmospheric Chemistry and Physics, 14, 10845-10895, 2014.

van Donkelaar, A., Martin, R. V., Brauer, M., and Boys, B. L.: Use of satellite observations for long-term exposure assessment of global concentrations of fine particulate matter, Environmental health perspectives, 123, 135, 2015.

Wang, J. X.: Mapping the Global Dust Storm Records: Review of Dust Data Sources in Supporting Modeling/Climate Study, Current Pollution Reports, 1, 82-94, 2015.

Wang, X., Heald, C., Ridley, D., Schwarz, J., Spackman, J., Perring, A., Coe, H., Liu, D., and Clarke, A.: Exploiting simultaneous observational constraints on mass and absorption to estimate the global direct radiative forcing of black carbon and brown carbon, Atmospheric Chemistry and Physics, 14, 10989-11010, 2014.

Wang, Y., Zhang, Q., He, K., Zhang, Q., and Chai, L.: Sulfate-nitrate-ammonium aerosols over China: response to 2000–2015 emission changes of sulfur dioxide, nitrogen oxides, and ammonia, Atmospheric Chemistry and Physics, 13, 2635-2652, 2013.

Yang, M., Howell, S., Zhuang, J., and Huebert, B.: Attribution of aerosol light absorption to black carbon, brown carbon, and dust in China–interpretations of atmospheric measurements during EAST-AIRE, Atmospheric Chemistry and Physics, 9, 2035-2050, 2009.

Ye, C., Zhang, N., Gao, H., and Zhou, X.: Photolysis of particulate nitrate as a source of HONO and NOx, Environmental Science & Technology, 2017. 2017.

Yu, F.: A secondary organic aerosol formation model considering successive oxidation aging and kinetic condensation of organic compounds: global scale implications, Atmospheric Chemistry and Physics, 11, 1083-1099, 2011.

Zender, C. S., Bian, H., and Newman, D.: Mineral Dust Entrainment and Deposition (DEAD) model: Description and 1990s dust climatology, Journal of Geophysical Research: Atmospheres (1984–2012), 108, 2003.

Zhang, L., Jacob, D., Knipping, E., Kumar, N., Munger, J., Carouge, C., Donkelaar, A. v., Wang, Y., and Chen, D.: Nitrogen deposition to the United States: distribution, sources, and processes, Atmospheric Chemistry and Physics, 12, 4539-4554, 2012.

Zhang, L., Kok, J. F., Henze, D. K., Li, Q., and Zhao, C.: Improving simulations of fine dust surface concentrations over the western United States by optimizing the particle size distribution, Geophysical Research Letters, 40, 3270-3275, 2013.

Zhang, Q., Jimenez, J., Canagaratna, M., Allan, J., Coe, H., Ulbrich, I., Alfarra, M., Takami, A., Middlebrook, A., and Sun, Y.: Ubiquity and dominance of oxygenated species in organic aerosols in anthropogenically-influenced Northern Hemisphere midlatitudes, Geophysical Research Letters, 34, L13801, 2007.

Zhu, L., Henze, D., Bash, J., Jeong, G.-R., Cady-Pereira, K., Shephard, M., Luo, M., Paulot, F., and Capps, S.: Global evaluation of ammonia bidirectional exchange and livestock diurnal variation schemes, Atmospheric Chemistry and Physics, 15, 12823-12843, 2015.

Zhu, L., Henze, D., Cady- Pereira, K., Shephard, M., Luo, M., Pinder, R., Bash, J., and Jeong, G. R.: Constraining US ammonia emissions using TES remote sensing observations and the GEOS- Chem adjoint model, Journal of Geophysical Research: Atmospheres, 118, 3355-3368, 2013.